HOUGHTON UNIVERSITY'S PHASE-SHIFTING LASER INTERFEROMETER FOR THE STUDY OF THIN METAL FILMS

By

Luke Yelle

A thesis submitted in partial fulfillment of the requirements for the degree of

Bachelor of Science

Houghton University

May 2025

Signature of Author…………………………………………………………………………………..

Department of Physics
May 5, 2025

……

Dr. Brandon Hoffman
Professor of Physics
Research Supervisor

……

Dr. Mark Yuly
Professor of Physics

HOUGHTON UNIVERSITY'S PHASE SHIFTING LASER INTERFEROMETER FOR THE STUDY OF THIN METAL FILMS

By

Luke Yelle

Submitted to the Department of Physics
on May 5, 2025, in partial fulfillment of the
requirement for the degree of
Bachelor of Science

Abstract

A modified Twyman-Green phase-shifting laser interferometer was built by Houghton University to determine the thickness of thin metal films. A 635 nm beam is split by a cube beam splitter. Lenses expand and culminate the beams to a diameter of 83 mm. One beam reflects off the thin film sample. The other reflects off a 10 cm diameter, $\frac{\lambda}{10}$ flat, phase-shifting reference mirror moving via piezoelectric ceramic stacks, controlled by an Arduino. Both are then combined to form an interference pattern on a screen. The intensity of a given point on the interference pattern changes sinusoidally with the change of position of the reference mirror. A set of pictures is taken at different reference positions by an HP high-definition camera and is then processed by a Processing code. Each pixel of the image set is fit to determine its effective intensity phase shift, which is then used to map the topography of the film surface.

Thesis Supervisor: Dr. Brandon Hoffman
Title: Professor of Physics

TABLE OF CONTENTS

Chapter 1 History of Light, Interferometry, and Thin Metal Films 5
1.1. Development and Support for a Particle Model of Light 5
1.1.1. Newton's Corpuscular Theory 5
1.1.2. The Photoelectric Effect 6
1.2. Development and Support for a Wave Model of Light 8
1.2.1. The Ether 8
1.2.2. Maxwell's Theory of Electromagnetic Waves 8
1.3. Light Interference 8
1.3.1. Light Interference 8
1.3.2. Young's Double Slit Experiment 10
1.4. Wave-Particle Duality 11
1.5. The Development of the Interferometer 11
1.5.1. The Michelson Interferometer 12
1.5.2. The Twyman-Green Interferometer 13
1.5.3. A Phase Shifting Interferometer 14
1.6. Thin Metal Films 15
1.7. Houghton University's Phase Shifting Interferometer 18

Chapter 2 Determining Film Thickness from an Interference Pattern 19
2.1. Electromagnetic Waves and Interference 19
2.1.1. 1D Wave Equation 19
2.1.2. Electric and Magnetic Fields as Sinusoidal Waves 21
2.1.3. Electric and Magnetic Field Proportionality 22
2.1.4. Electric and Magnetic Fields are Perpendicular 23
2.1.5. Intensity - The Poynting Vector 24
2.1.6. Interference 24
2.2. Determining Film Thickness 26
2.2.1. Determining the Effective Wave Number 28
2.2.2. Determining the Effective Phase Shift 29
2.2.3. Calculation of Film Thickness 31

Chapter 3 Houghton University's Interferometer 33
3.1. Houghton University's Phase Shifting Laser Interferometer 33
3.2. Phase Shifting Mirror 35
3.2.1. Hardware 35
3.2.2. Ramp Circuit 36
3.2.3. The Interference Pattern 36
3.3. Data Analysis Code 37
3.3.1. Determining Intensity 37
3.3.2. Finding the Effective Phase Shift 39

Chapter 4 Conclusion 40

TABLE OF FIGURES

Figure 1. Reflection and Refraction. 6
Figure 2. The photoelectric effect. 7
Figure 3. Light Interference. 9
Figure 4. The Double Slit Experiment Results. 10
Figure 5. The Michelson Interferometer. 13
Figure 6. Twyman-Green Interferometer 14
Figure 7. Phase Shifting Interferometer 15
Figure 8. Transformation from <111> to <100> 16
Figure 9. Thickness dependence on atomic transformation. 17
Figure 10. Light Interference 26
Figure 11. The Interference Pattern. 27
Figure 12. Thin Film sample. 32
Figure 13. Setup of Houghton's modified Twyman-Green Interferometer. 34
Figure 14. Houghton University's Interferometer 35
Figure 15. Reference Mirror. 36
Figure 16. Systematic Diagram of the ramp circuit. 37
Figure 17. Changing the interference pattern as the mirror shifts. 38
Figure 18. Intensity vs. image. 38

Chapter 1

HISTORY OF LIGHT, INTERFEROMETRY AND THIN METAL FILMS

1.1. Development and Support for a Particle Model of Light

There has been a century-long debate about the nature of light: whether it behaves like a particle or a wave. While both perspectives have experimental support, the wave-like behavior of light is particularly important for interferometry. This section will briefly review some key theories and experiments that support the particle-like description of light, but the focus will shift to those that reveal its wave-like nature. Understanding light as a wave is essential, as it is this property that allows for the interference patterns central to interferometry.

1.1.1. Newton's Corpuscular Theory

In 1730, Sir Isaac Newton developed one of the first theories of light. His theory explains light as a particle, which he calls a "corpuscle". His three-book treatise [1], describes how these minuscule, massless particles always travel in straight lines, where light can reflect off mediums and refract when changing mediums. These phenomena are explained in Figure 1.

Reflection occurs when light hits a medium and bounces off it. When the light hits perpendicularly, it returns with equal momentum in the opposite direction. If it hits the medium at an angle, it will reflect at the same angle while keeping the same momentum parallel to the mirror. That is, the angle of incidence equals the angle of reflection.

Refraction occurs when light travels from one medium to another. Newton theorized that when light refracts, it experiences an added force from the medium, changing its speed and direction. We now know that when going into a less dense medium, the speed of light is greater, and the angle of incidence is less than the angle of reflection. When going into a denser medium, it switches, becoming slower and having a greater angle of refraction.

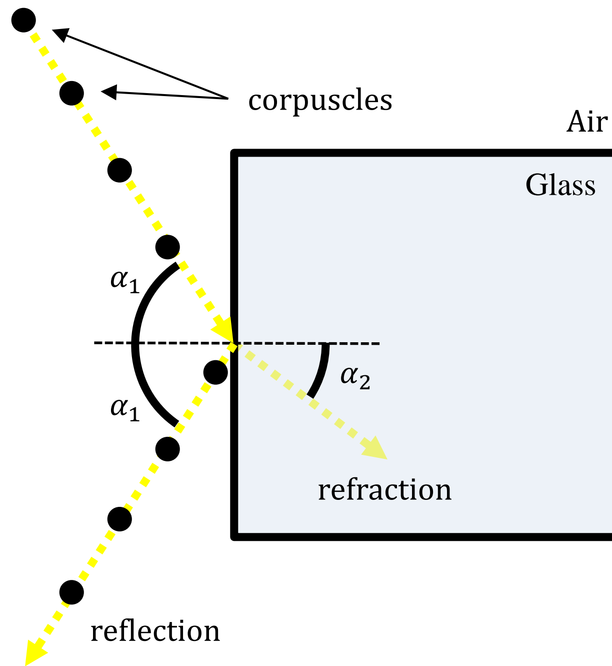

Figure 1. Reflection and Refraction. Sir Isaac Newton used the concepts of reflection and refraction to explain light as a particle. When light reflects off of a medium barrier, the light can reflect off of the surface at the same angle relative to the normal, or the dotted black line. (the angle of incidence equals the angle of reflection). This is a particle-like phenomenon. The light can also change mediums through refraction. This changes the angle relative to the normal so that the denser medium has a smaller angle (the angle of incidence α_1 is is greater than the angle of refraction α_2). The speed of the light also slower in denser mediums, which is a phenomenon that occurs with particles.

Because particles travel in straight lines unless an external force acts on them, light travelling in this way can express its particle-like nature. Gradually over the next century, however, the wave theory of light took over as the leading theory of the nature of light. In the late 1800s, the photoelectric effect experiment tested the theory, which states that light can be described as a particle.

1.1.2. The Photoelectric Effect

Heinrich Hertz published the first work [2] on a now-famous experiment studying the properties of light in 1887. The experiment supported the idea of light acting like a particle, even though Hertz initially studied electromagnetic waves, a wave theory of light that dominated the scientific world.

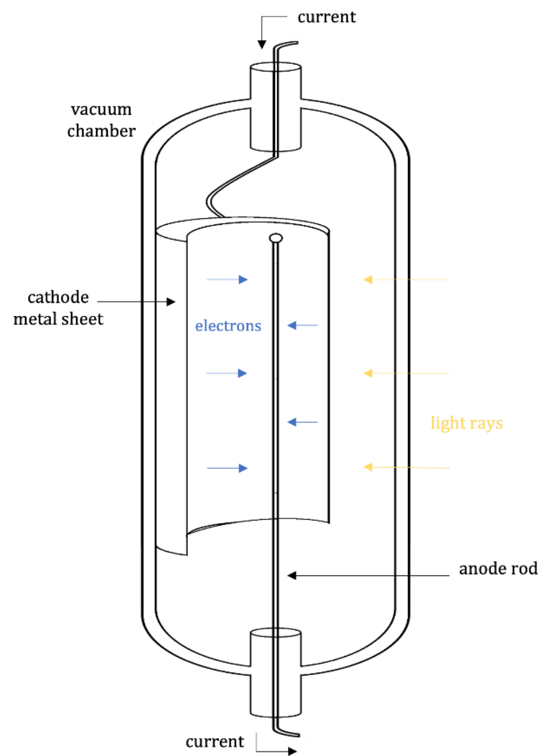

Figure 2. The photoelectric effect. Above is a remade version of the photoelectric effect experiment that Hertz conducted. When light rays hit the cathode metal sheet, electrons were excited and pulled free from the metal plate, then attracted to the anode, allowing current to flow. The electrons were only ejected when the light surpassed a certain frequency, suggesting that the light hitting the metal had particle-like properties.

Hertz's apparatus, visually explained in Figure 2, had a monochromatic light source shine onto a metal plate, which acted as a cathode, to excite and free electrons. Due to the potential difference between the cathode and the anode, the electrons were attracted to the anode. A detector on the anode measured the energy of the electrons as they bombarded it. This is all done within a vacuum chamber to limit the energy lost from the particles between the cathode and anode.

In Einstein's paper written in 1905 [3], he shared how light is an energized particle, which he called photons. Particles of light similar to corpuscles. When the photons hit the cathode in the photoelectric effect experiment, the electrons were observed to only be ejected when the frequency of the light was greater than some value, suggesting that the frequency gave a quantized amount of energy and not a continuous stream of energy.

1.2. Development and Support for a Wave Model of Light

1.2.1. The Ether

In 1665, Christiaan Huygens [4] was one of the first to present an alternate theory to partially explain Newton's prism experiment, made to support the theory of light as a particle. Huygens developed a wave theory of light to explain how light reflects and refracts. He built his theory upon ideas from Robert Hooke and his theory of light [5] being a wave that propagates through a medium he called the "ether".

He developed a principle that every point on a wavefront acts as a source for later wavefronts. This idea can be explained as a rock thrown into a lake or pond with perfectly still water. When it is thrown into the water, the waves formed move away from the source in all directions, where each wavefront is created from the previous wavefront.

1.2.2. Maxwell's Theory of Electromagnetic Waves

Maxwell's theory [6] was fundamental to the development of the wave-like nature of light. At this point there had already been experiments done such as Youngs double slit experiment to explain the wave nature of light, however the cause of the wave and what makes up the wave was still unknown. In the late 1860s, Maxwell took a collection of experimentally supported mathematical expressions for electric and magnetic fields and related them to explain how light could work as a collection of these two waves, or an electromagnetic wave.

His theory, originally published in 1861, explained using a mechanical model from the concept of "lines of force" [7], introduced by Michael Faraday [8]. The lines of force explained how electric and magnetic fields propagate through space. Four years later, in 1865, Maxwell updated his theory. He used the mathematical laws derived by Charles-Augustin de Coulomb [9], André-Marie Ampère [10], Carl Friedrich Gauss [11], and Faraday to determine the speed of light using electric and magnetic fields, thus explaining light as an electromagnetic wave.

1.3. Light Interference

1.3.1. Light Interference

Light's wave-like nature is useful to describe the phenomenon when two light beams interact with each other. When two light beams cross each other's path, an electromagnetic light

wave is formed. This wave is a disturbance that has a magnitude and direction. When two or more disturbances overlap (interfere), the result is a simple vector sum of the independent disturbances. If the sum is larger than the individuals, the interference is considered to be constructive. Otherwise, it is destructive. The oscillating electric and magnetic fields create a light wave, so the constructive interference is the greatest when the peaks of the two individual waves coincide. Figure 3 explains the superposition of the light waves, creating a high intensity point at the places where two light peaks match up. The more the peaks overlap, the greater the intensity.

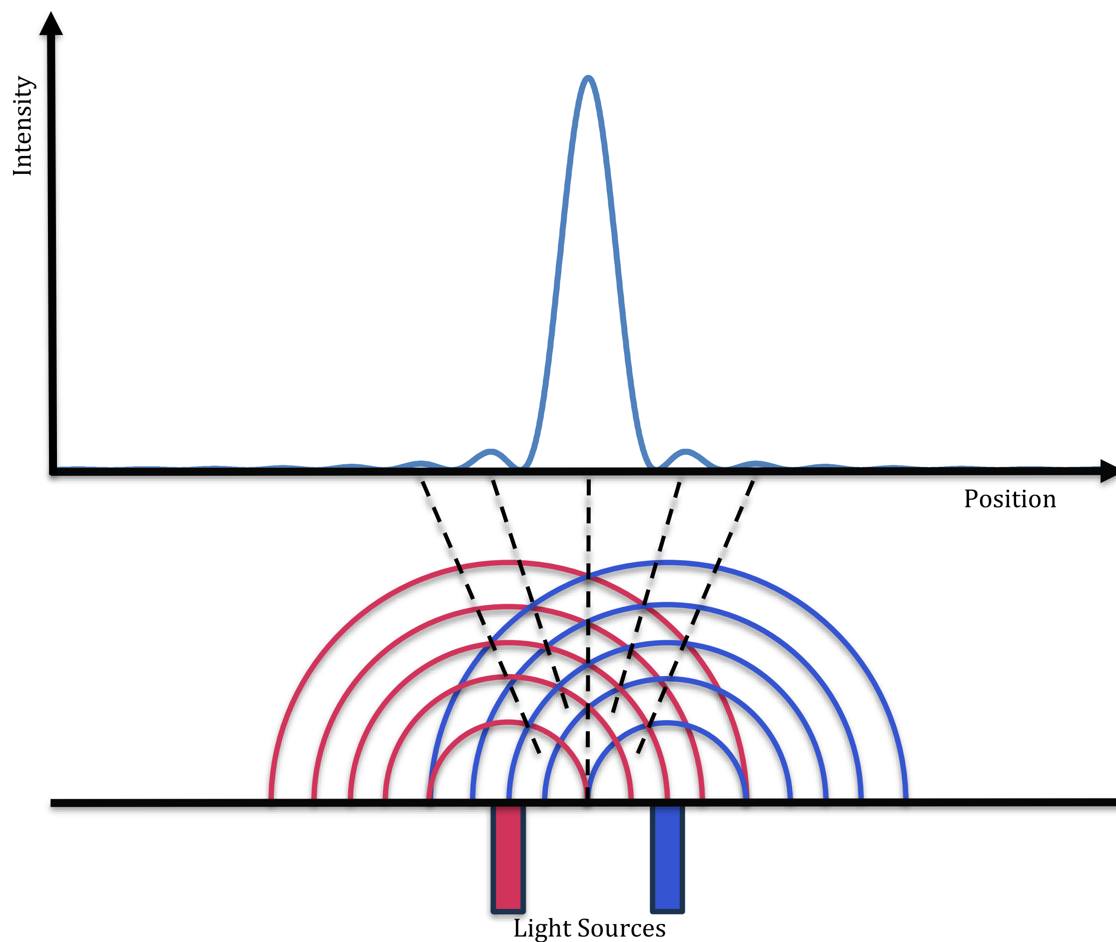

Figure 3. Light Interference. The wavefronts going in all directions from each light source allow for constructive and destructive interference along each wavefront. The intensity of the resulting interference pattern displayed on the screen is plotted above. The dashed lines represent the interference in each wavefront as the light propagates through the space between the light source and the screen. The relative intensity of each peak results from interference between waves from all the points along one of the slits. Note that the colors of the light are just differentiating between the two sources.

Other than the point with the greatest intensity, there is a difference in distance between the two light sources. This is called a path length difference, and it results in the two wave fronts being out of phase. In Figure 4, the path length difference is shown for a peak intensity with a path length difference between the two light sources. At this point, the light constructively interferes to create a peak, meaning that the phase shift is at a multiple of the period.

1.3.2. Young's Double Slit Experiment

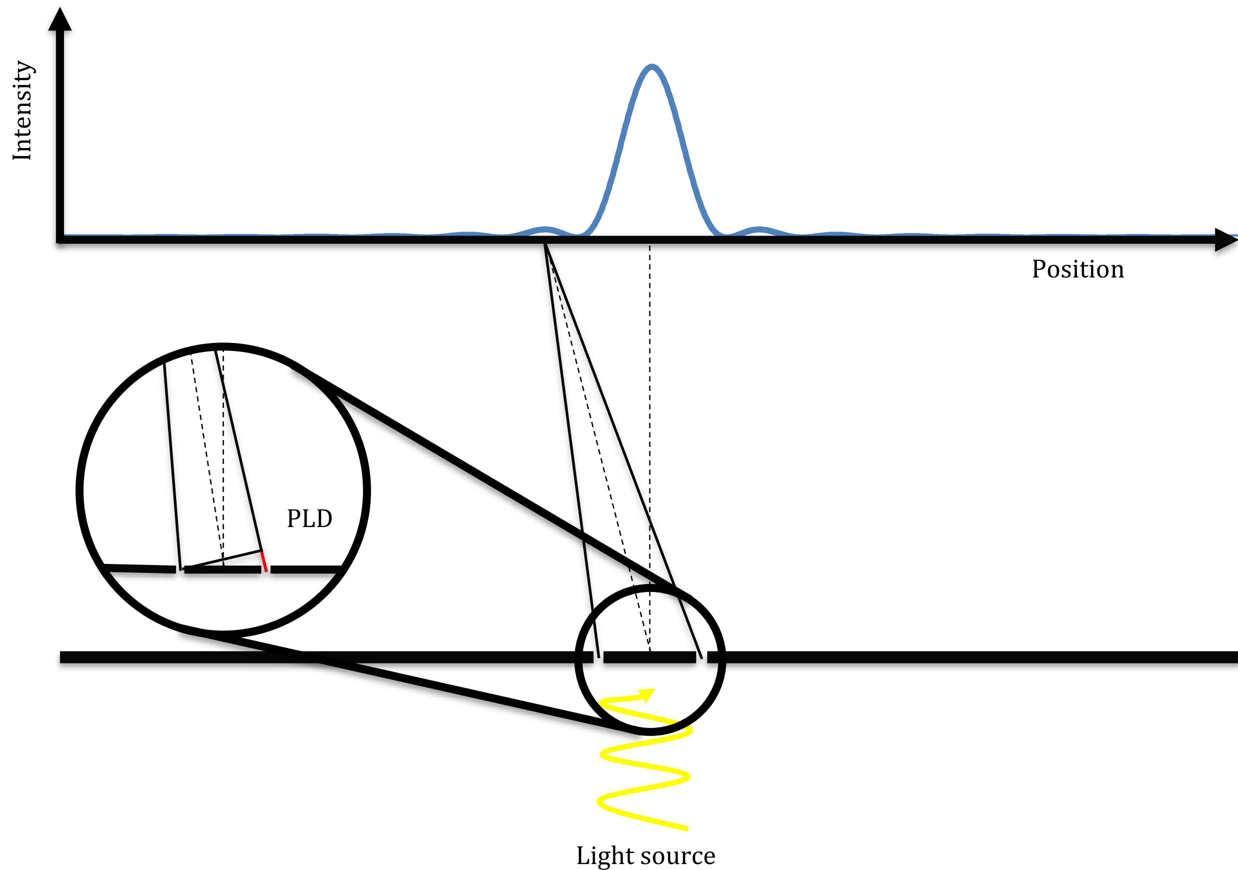

Figure 4. The Double Slit Experiment Results. When conducting the double slit experiment, a wave function was shown on the screen. This must be because of light acting like a wave, where the light expands from the slit in every direction like a wave, and then the light from one slit interferes with the light coming from the other slit, creating areas of low light intensity and high light intensity.

Young's experiments with light interference [12] are extremely useful experiments to support the wave model. His experiment, publicly demonstrated during lectures, used a

mirror, a hole in a window shutter, and a strip of card, as shown in Figure 4. The strip of card was put across the hole to create two separate holes. He observed alternating fringes on the screen, meaning the lights interfered with each other as they propagated through the air after going through the slits in the card.

1.4. Wave-Particle Duality

Due to the experiments supporting the particle theory and the wave theory of light, Albert Einstein began to develop a new understanding of light's nature. He theorized that light could behave both like a wave and like a particle, introducing the idea of wave-particle duality. Einstein's work on the photoelectric effect provided strong evidence for this duality. Classical wave theory developed by Maxwell and his equations treated light as a continuous electromagnetic wave, meaning its energy should spread out smoothly over space. However, Einstein pointed out a contradiction in this view. Many phenomena, such as the photoelectric effect, could not be explained through electromagnetic waves. Energy from a wave would provide a continuous stream of energy, instead of the quantized amount of energy seen in the experiment. To resolve this, Einstein proposed in his 1905 paper [3] that light consists of discrete packets of energy called photons. Each photon carries energy proportional to its frequency, expressed as

$$E = hf, \tag{1}$$

with E being the energy of the photon, h is Planck's constant, and f is the frequency of the light. It explains the energy of a photon. It gives a quantized energy state and relates the energy to the frequency of the photon. This frequency explains the wave-like properties of the photon, where it oscillates like a wave and propagates like a wave. Interferometry uses the wave nature of light, like Maxwell's electromagnetic waves, and light interference to determine the thickness of thin metal films.

1.5. The Development of the Interferometer

Interferometry is a technique used to measure extremely small distances. There are numerous variations of interferometers, with many using light interference to determine

this distance by reflecting a light source off of a reference point and the measured sample, then analyzing the interference pattern created when the two light sources meet.

1.5.1. The Michelson Interferometer

The Michelson Interferometer [13] is the first interferometer, built in 1881 [14] by Albert Michelson to measure the speed of light. His interferometer was a creation used for the Michelson-Morley experiments, a series of experiments that tried to measure the rotation of the Earth using the propagation of the light through the ether. The experiment depicted in Figure 5 had a single slit to let light travel collimated to a large glass optical flat silvered mirror that reflected half of the light and let half transmit through it. This acted as a beam splitter. The two light beams would reflect off mirrors set to be perpendicular to the direction of the beam, so that the light will reflect back to the beam splitter. The mirrors were set up to be the same distance away from the beam splitter. The combined light would shin on a viewing screen which allowed the viewer to see the interference created from the two beams. Since the two mirrors were the same distance away from each other, there should be no light interference, and the light intensity should be the same as how it started. However, Michelson believed that if the apparatus was oriented in a certain way, the motion of the Earth through the ether could be measured. A shift in the interference pattern was expected when the apparatus was rotated, however no change was measured.

The experiments conducted by Michelson did not succeed in detecting the Earth's motion through the ether. However, the Michelson-Morley experiments played a crucial role in refuting the theory that a medium like the ether must exist for light to propagate. The Michelson interferometer was essential for demonstrating the constant speed of light [15]. By measuring the slight time difference, it takes light to travel along the two difference paths (a-b-a versus a-c-a), these variations could be observed through the resulting interference pattern. Using the known distances between the beam splitter and the mirrors as well as the measured time difference, the speed of light could be accurately calculated. The Michelson interferometer was not only a groundbreaking tool during his own lifetime of research, but it also laid the foundation for future experiments and interferometer designs. The design has

been improved and altered leading to variations of the interferometer, such as the Twyman-Green interferometer.

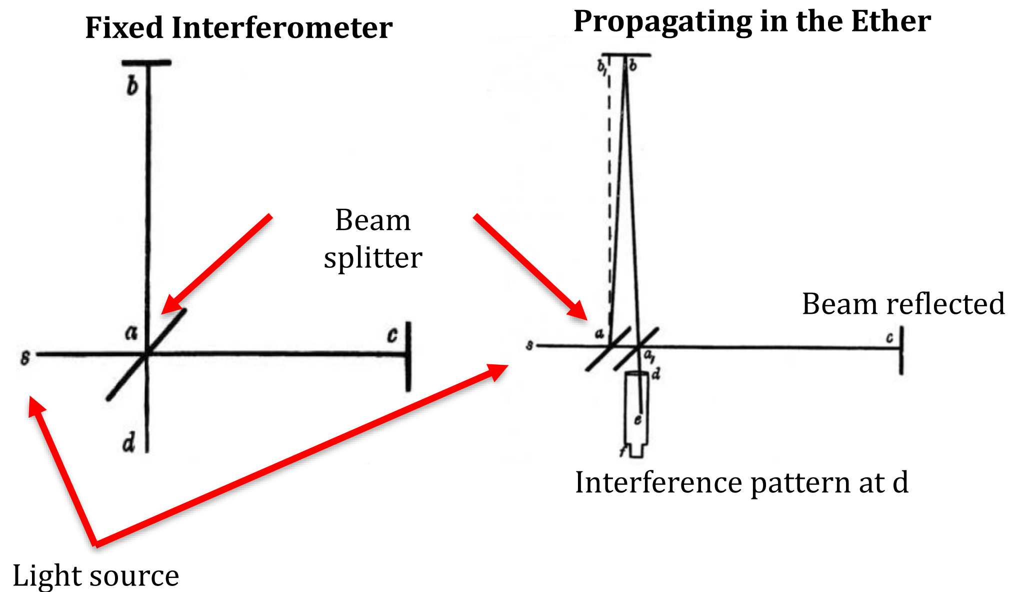

Figure 5. The Michelson Interferometer. The left indicates a simplified diagram of the points of contact for the light. Point s is the light source. It is directed towards a beam splitter at point a. The light is split and goes towards points c and b, and then is reflected to a, and then recombined at point d. Point d is a telescope used for observation. The right side is how Michelson predicted how the light propagated through the ether relative to the position of the points from the left. The rotation of the Earth is to the right. So, when the light reflects off of points b and c, they return to point a1, where the propagation of the ether relative to the motion of the Earth is measured. However, it is important to note the motion of the Earth was never measured using this method. The experiment gave a very important null result. However, it led to the determination of the speed of light. This device is also the stepping stone to many experiments modifying the interferometer. Figure partially taken from Ref. [13].

1.5.2. The Twyman-Green Interferometer

Frank Twyman and Arthur Green modified Michelson's interferometer in 1916 to accomplish a new measurement [16]. This interferometer took the template of dividing a light source and comparing the path length difference, and used lenses to diverge the light and observe a full surface topography. The adaptation was for the purposes of optical testing.

Figure 6 depicts the apparatus. The same setup of a white light source that split a beam splitter into two beams each going down an arm. One beam was directed a flat reference

mirror – made as flat as possible to limit error – and the other beam reflected off an optical surface that was being tested. The idea of Twyman and Green's experiments were to study the interference pattern created by the path length difference between the two light beams. The surface being studied was concave so that each point had a similar path length difference from the diverging lens, other than deformities in the surface (such as cuts or bumps that are being measured through the interference pattern).

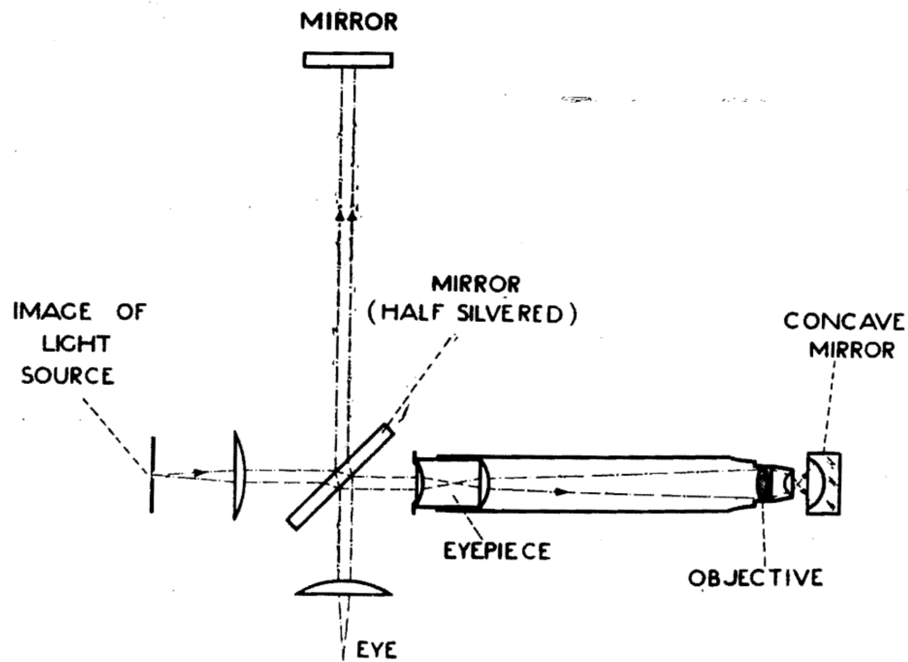

Figure 6. Twyman-Green Interferometer. This is similar to the Michelson Interferometer, where a light source is directed to a beam splitter. One beam then hits a mirror and then returns to the beam splitter. The other beam diverges and hits a concave mirror with the objective on it. This objective is what is being measured using the interference pattern viewed from the eye. Figure taken from Ref. [17].

1.5.3. A Phase Shifting Interferometer

Like a Twyman-Green Interferometer, phase-shifting interferometers make precise measurements using mirrors and lenses; however, they also incorporate a shifting mirror so that many different interference patterns are created on the screen. Many variations of this type of interferometer have been made, with one being shown in Figure 7. In 1993, the

National Physics Lab built a primary length bar interferometer in Teddington, England. The interferometer made absolute value measurements of precision steel "length bars", steel bars of 22 mm diameter that are the standard length for the metric system used in laboratory and manufacturing environments. The phase-shifting mirror moved one-eighth of a wavelength for each picture, slightly changing the interference pattern shown on the screen. The interference pattern changes sinusoidally as the mirror moves away from the beam splitter. By taking images at various phase steps, the phase shift can be measured more accurately due to the ability to average out noise, reduce sensitivity to environmental disturbances, and extract precise phase information from multiple intensity measurements. This interferometer can be obtained within 20 nm of the target length. This kind of interferometer helps to determine minute differences in distance, even more than the Twyman-Green Interferometer. It is required when studying something like thin metal films.

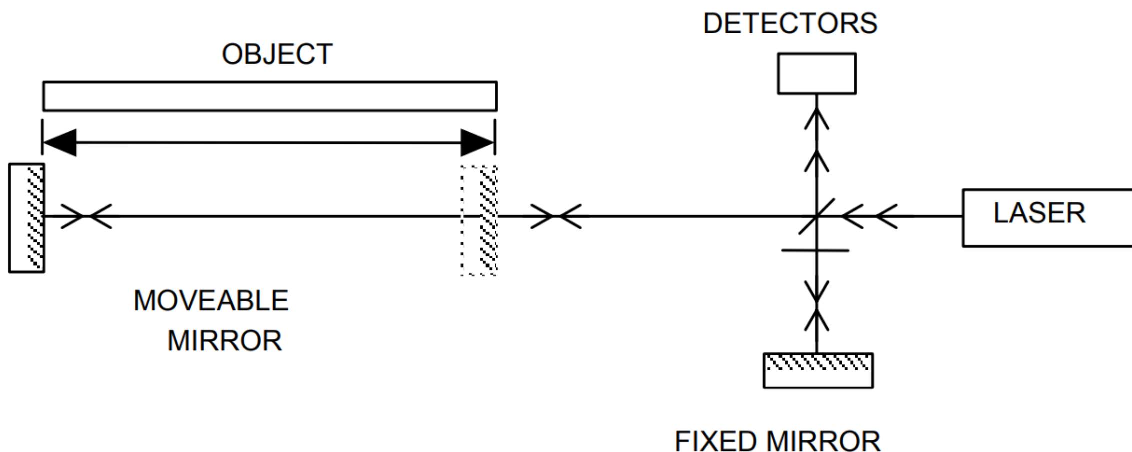

Figure 7. Phase Shifting Interferometer. This is the same layout as the Michelson or the Twyman-Green Interferometer, however, now the reference mirror is made to move several hundred nanometers during imaging. This allows for multiple phase shifts in the light. Figure taken from Ref. [18].

1.6. Thin Metal Films

Thin metal films are devices that are small in one dimension relative to the other. This results in a metal film that typically has a thickness on the order of micrometers or less. These thin

metal films are used in a variety of technologies such as solar panels, computer chips, and circuit boards. They are devices that are important in the field of optics, used for coatings of screws and other tools, and are used in various microelectronics.

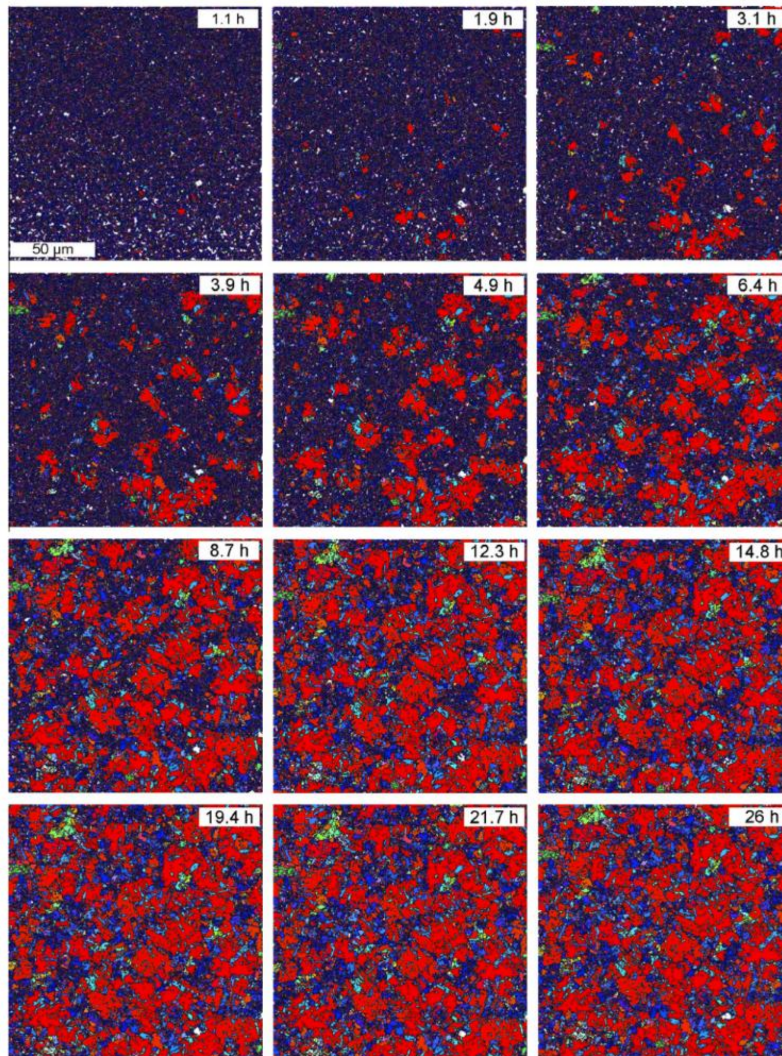

Figure 8. Transformation from <111> to <100>. The blue represents the <111> atomic configuration, and the red represents the <100> atomic configuration. The figure represents the film as it is being annealed over 24 hours. The film starts with almost all <111>, but after 24 hours, more than half of the structures in the film are transformed into <100>. Figure taken from Ref [19]

When a metal is deposited on a silicon substrate, it forms a polycrystalline film, with crystallites oriented in a variety of directions relative to the film surface. If much of the film consists of grains oriented in one direction, the film is said to have a strong texture. During

heating cycles, atoms move from one crystallite to another, causing some crystallites to grow large. If these have a different orientation than that of the original texture, the film will have a new texture. For example, Figure 8 shows an Ag thin film produced at Cornell University and imaged by students at Houghton University. The film originally consists almost entirely of (111)-oriented crystallites, tens of nanometers in diameter. As the film is annealed, (100)-oriented crystallites grow until they are as much as 40-50 μm wide.

The amount of texture transformation depends on the thickness of the. Figure 9 shows the results of x-ray diffraction measurements [20] made by Houghton University students at Cornell from Ag films similar to the ones shown in Figure 7. The plots in Figure 9 show the percentage of the film oriented in the (111) direction after one hour of annealing. The texture of the films greater than about 1.5 nanometers thick readily transformed. However, the texture of films less than 1.0 nanometers thick did not transform. Although this phenomenon has been well documented, the cause remains unknown.

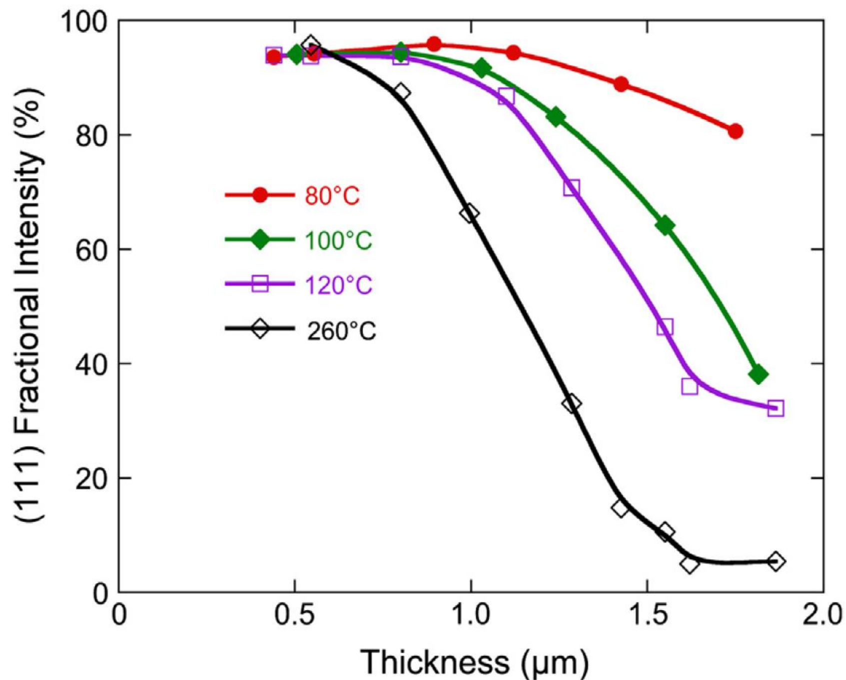

Figure 9. Thickness dependence on atomic transformation. The original structure of the deposited atomic crystal is (111), which is partially transformed upon annealing to an atomic structure (100). As the thickness of the film increases, the percentage of (111) still on the film after annealing decreases. Plot taken from Ref [20]

1.7. Houghton University's Phase Shifting Interferometer

At Houghton University, a modified Twyman-Green phase-shifting laser interferometer is being developed to determine the thickness of thin metal films that we create. Lenses collimate the beams at 83 mm diameter. Images of the interference pattern are taken at roughly 100 positions of the phase-shifting reference mirror. The set of images is processed pixel by pixel to produce a nanometer height resolution topography of the sample surface. From that, the thickness of the film will be determined.

Chapter 2

DETERMINING FILM THICKNESS FROM AN INTERFERENCE PATTERN

2.1. Electromagnetic Waves and Interference

2.1.1. 1D Wave Equation

One of the most prominent theories of light is Maxwell's theory [6,7] that light is made of electromagnetic waves. Electric and magnetic fields were already explained through equations such as Ampere's Law and Gauss' Law. Maxwell used these equations to explain the relationship between the electric and magnetic fields. These equations are now called Maxwell's equations and are used to develop the electromagnetic wave theory of light. A changing electric field produces a magnetic field and vice versa. This results in the formation of light as explained through the equations.

Faraday's law gives a relationship between the electric field and the rate of change of the magnetic field, shown as

$$\vec{\nabla} \times \vec{E} = -\frac{\partial \vec{B}}{\partial t}, \tag{2}$$

with $\vec{E}$ representing the electric field and $\vec{B}$ representing the magnetic field. Faraday's Law expresses that a changing magnetic field induces an electric field. Taking the curl of each gives a relationship of

$$\vec{\nabla} \times \left(\vec{\nabla} \times \vec{E}\right) = \vec{\nabla}\left(\vec{\nabla} \cdot \vec{E}\right) - \nabla^2 \vec{E} = -\frac{\partial}{\partial t}\left(\vec{\nabla} \times \vec{B}\right). \tag{3}$$

Gauss's Law for the electric field

$$\vec{\nabla} \cdot \vec{E} = \frac{\rho}{\varepsilon_0} \tag{4}$$

can be used to simplify the left side of Equation (3), where ρ represents the charge density and ε_0 represents the permittivity of free space. The Ampere-Maxwell Law

$$\vec{\nabla} \times \vec{B} = \mu_0 \varepsilon_0 \frac{\partial \vec{E}}{\partial t} + \mu_0 \vec{J}, \tag{5}$$

where μ_0 represent the permeability of free space and $\vec{J}$ is the current density, is another relationship that helps to simplify the right side of Equation (3). In a case where there is no charge or current (which is what we expect for electric and magnetic fields in free space), it is simplified to

$$\nabla^2 \vec{E} = \mu_0 \varepsilon_0 \frac{\partial^2 \vec{E}}{\partial t^2}, \tag{6}$$

representing the wave equation for the electric field. The wave equation explains how an electric field propagates through space like a wave. For a laser, all the light is collimated and uniformly perpendicular to the direction of propagation, meaning that the electric field only has a dependence on z (a dimension in space), not on x or y. The electric field can be represented as

$$\vec{E}(z,t) = E_x(z,t)\hat{\imath} + E_y(z,t)\hat{\jmath} + E_z(z,t)\hat{k}, \tag{7}$$

where x, y and z are coordinates in space. Substituting this into Equation (6) results in a plane wave:

$$\frac{\partial^2 \vec{E}}{\partial z^2} = \mu_0 \varepsilon_0 \frac{\partial^2 \vec{E}}{\partial t^2}. \tag{8}$$

A similar process can be done to derive the wave equation for the magnetic field, starting with Ampere's Law with no current and taking the curl of each side of the equation, leading to

$$\vec{\nabla} \times (\vec{\nabla} \times \vec{B}) = \vec{\nabla}(\vec{\nabla} \cdot \vec{B}) - \nabla^2 \vec{B} = \mu_0 \varepsilon_0 \frac{\partial}{\partial t}(\vec{\nabla} \times \vec{E}). \tag{9}$$

Simplifying the left side of Equation (9) using Faraday’s Law from Equation (2), and Gauss’s Law of Magnetism,

$$\vec{\nabla} \cdot \vec{B} = 0, \tag{10}$$

gives a relationship similar to Equation (6):

$$\nabla^2 \vec{B} = \mu_0 \varepsilon_0 \frac{\partial^2 \vec{B}}{\partial t^2}. \tag{11}$$

Assuming a magnetic field of

$$\vec{B}(z,t) = B_x(z,t)\hat{\imath} + B_y(z,t)\hat{\jmath} + B_z(z,t)\hat{k}, \tag{12}$$

the plane wave equation for the magnetic field

$$\frac{\partial^2 \vec{B}}{\partial z^2} = \mu_0 \varepsilon_0 \frac{\partial^2 \vec{B}}{\partial t^2}. \tag{13}$$

is determined. The constant $\mu_0 \varepsilon_0$ can be represented as

$$\mu_0 \varepsilon_0 = \frac{1}{c^2}. \tag{14}$$

Because the 1D wave equation for the electric and magnetic fields can be derived from Maxwell's equations, both fields can be represented by a sinusoidal function.

2.1.2. Electric and Magnetic Fields as Sinusoidal Waves

Equations (8) and (13) represent the electric and magnetic fields as a 1D plane wave. The solutions for the electric field's 1D wave equation is

$$\vec{E}(z,t) = \vec{f}(z - vt) + \vec{g}(z + vt). \tag{15}$$

where $\vec{f}(z - vt)$ is a right-moving wave and $\vec{g}(z + vt)$ is a left-moving wave. The velocity of the wave is represented by v. The geometry of light travelling from a source to a detector can be defined such that

$$\vec{g}(z + vt) = 0. \tag{16}$$

But what is $\vec{f}(z-vt)$? This can be determined through a Fourier Transform. $\vec{f}(z-vt)$ is a function of many different plane waves, each with a different spatial frequency, k. To collect all possible plane waves, one must integrate over all space with respect to k. An inverse Fourier Transform is represented as

$$\vec{f}(t)=\int_{-\infty}^{\infty}\vec{P}(k)\sin kt+\vec{Q}(k)\cos kt\,dk \quad (17)$$

To use this for the electric field 1D wave equation, replace $\vec{f}(t)$ with $\vec{f}(z-vt)$, and the kt in the exponent with $kz-\omega t$, where $\omega=vk$. When this is done, the transform becomes

$$\vec{f}(z-vt)=\int_{-\infty}^{\infty}\vec{P}(k)\sin(kz-\omega t)+\vec{Q}(k)\cos(kz-\omega t)\,dk \quad (18)$$

where $\vec{P}(k)$ and $\vec{Q}(k)$ are Fourier amplitudes, or how much k is present. The origin of the z-axis can be defined such that $\vec{f}(z-vt)=0$ when $z=0$. Therefore, $\vec{Q}(k)$ will equal zero, and for the electric and magnetic fields, the resulting solutions will be

$$\vec{E}(z,t)=\vec{E}_0\sin(k_Ez-\omega_Et+\phi_E) \quad (19)$$

and

$$\vec{B}(z,t)=\vec{B}_0\sin(k_Bz-\omega_Bt+\phi_B), \quad (20)$$

where $\vec{E}_0$ and $\vec{B}_0$ are constants, k is the wave number (or $2\pi/\pi$), ω represents the angular frequency ($\omega=2\pi f$ with f being frequency), and ϕ_E and ϕ_B are effective phase shifts of the field's wave.

2.1.3. Electric and Magnetic Field Proportionality

Maxwell's equations can also express the proportionality of the magnetic and electric fields. For the same electric field expressed in the Equation (7), with no charge or current, Gauss's Law for electricity can be simplified to find that the electric field, assuming no charge, is

$$\vec{\nabla} \cdot \vec{E}(z,t) = \frac{\partial E_x(z,t)}{\partial x} + \frac{\partial E_y(z,t)}{\partial y} + \frac{\partial E_z(z,t)}{\partial z} = \frac{\partial E_z(z,t)}{\partial z} = 0. \tag{21}$$

Because the electric field is only a function of z, the first two terms are zero, leaving the derivative of E_z with respect to z. Because of this, $E_z = E(t)$, meaning the z component is uniform through space.

Similarly, for a magnetic field expressed in the Equation (13),

$$\begin{aligned}\vec{\nabla} \times \vec{B}(z,t) &= \frac{\partial B_y(z,t)}{\partial z}(-\hat{\imath}) + \frac{\partial B_x(z,t)}{\partial z}\hat{\jmath} \\ &= -\mu_0\varepsilon_0\left(\frac{\partial E_x(z,t)}{\partial t}\hat{\imath} + \frac{\partial E_y(z,t)}{\partial t}\hat{\jmath} + \frac{\partial E_z(t)}{\partial t}\hat{k}\right).\end{aligned} \tag{22}$$

Comparing the $\hat{k}$ components gives

$$\frac{\partial E_z(t)}{\partial t} = 0. \tag{23}$$

Putting this all together, E_z is constant over all time and all space. It cannot create a light wave because it can only be made through a changing electric field over time and space. For mathematical convenience, set $E_z = 0$.

Similarly to the electric field, using Gauss's Law for Magnetism and Faraday's Law, the z component of the magnetic field is a constant. Because B_z does not vary in space or time, it does not concern light waves. So, set $B_z = 0$.

Equation (22) can only be true for all time and space if $k_E = k_B$, $\omega_E = \omega_B$, and $\phi_E = \phi_B$. Defining these terms as k, ω and ϕ gives

$$|\vec{E}| \propto |\vec{B}|. \tag{24}$$

2.1.4. Electric and Magnetic Fields are Perpendicular

Using Faraday's Law, a relationship between an electric and magnetic field can be made when the fields are represented with the equations expressed in (19) and (20), which looks like

$$\hat{k} \times \vec{E} = \frac{\omega}{k}\vec{B}. \tag{25}$$

Thus, the electric field is perpendicular to the magnetic field, and $|\vec{E}| \propto |\vec{B}|$ with the proportionality constant between the fields being ω/k.

2.1.5. Intensity - The Poynting Vector

The Poynting Vector is a value that gives the magnitude and direction of the electromagnetic wave based on the magnetic and electric fields that create the light wave. The Poynting Vector gives intensity and the direction of the light. The Poynting Vector, $\vec{S}$, is expressed as

$$\vec{S} = \frac{1}{\mu_0}\vec{E} \times \vec{B}. \tag{26}$$

Because the electric field is both proportional and perpendicular to the magnetic field, the Poynting Vector's magnitude can be represented as

$$|\vec{S}| \propto |\vec{E}|^2. \tag{27}$$

The time average of $|\vec{S}|$ gives the average intensity of light, meaning it is the light that is seen. So, the electric field's magnitude correlates with the intensity of light that is shown in any location.

2.1.6. Interference

When two electromagnetic waves interfere, the result is a vector sum of the two, which is itself a wave. If the amplitude is smaller than the individual waves, it is called destructive. if bigger, it is constructive. Say that two electromagnetic waves interfere with the same frequency and amplitude, but with different effective phase shifts. Figure 10 is a visual depiction of this interference. Have the first wave be

$$\vec{E}_1(z,t) = \vec{E}_0 \sin(kz - \omega t + \phi_1) \tag{28}$$

and the second wave be

$$\vec{E}_2(z,t) = \vec{B}_0 \sin(kz - \omega t + \phi_2). \tag{29}$$

When the two interfere, the resulting wave is

$$\vec{E}_{total}(z,t) = \vec{E}_0(\sin(kz - \omega t + \phi_1) + \sin(kz - \omega t + \phi_2)). \tag{30}$$

Using trigonometric identity

$$\sin(\theta) + \sin(\beta) = 2\sin\left(\frac{\theta + \beta}{2}\right)\cos\left(\frac{\theta - \beta}{2}\right) \tag{31}$$

Equation (29) can be simplified to

$$\vec{E}_{total}(z,t) = 2\vec{E}_0 \cos\left(\frac{\phi_2 - \phi_1}{2}\right)\sin\left(kz - \omega t - \frac{\phi_2 + \phi_1}{2}\right), \tag{32}$$

where $2\vec{E}_0 \cos\left(\frac{\phi_2 - \phi_1}{2}\right)$ is the amplitude of the wave. Thus, the amplitude of that wave is determined only by the difference $\Delta\phi = \phi_2 - \phi_1$.

The intensity of the resulting wave is the amplitude of the electric field, as explained in Equation (27), and can be expressed as

$$\langle|\vec{S}|\rangle = I(z) \propto \left|\vec{E}_1(z,t) + \vec{E}_2(z,t)\right|^2 \tag{33}$$

where the intensity of $\vec{E}_{total}$ is

$$I(z) \propto \left|\cos\left(\frac{\phi_2 - \phi_1}{2}\right)\right|^2. \tag{34}$$

When it comes to the interferometer, the effective phase shift in the wave is created due to a path length difference that the light has to go through after being split by the beam splitter. The path length consists of two distances: the position of the average plane of the sample and the distance from that plane to the point of reflection (topography of the thin film sample). The difference in distance travelled (or path length) results in the effective phase shift.

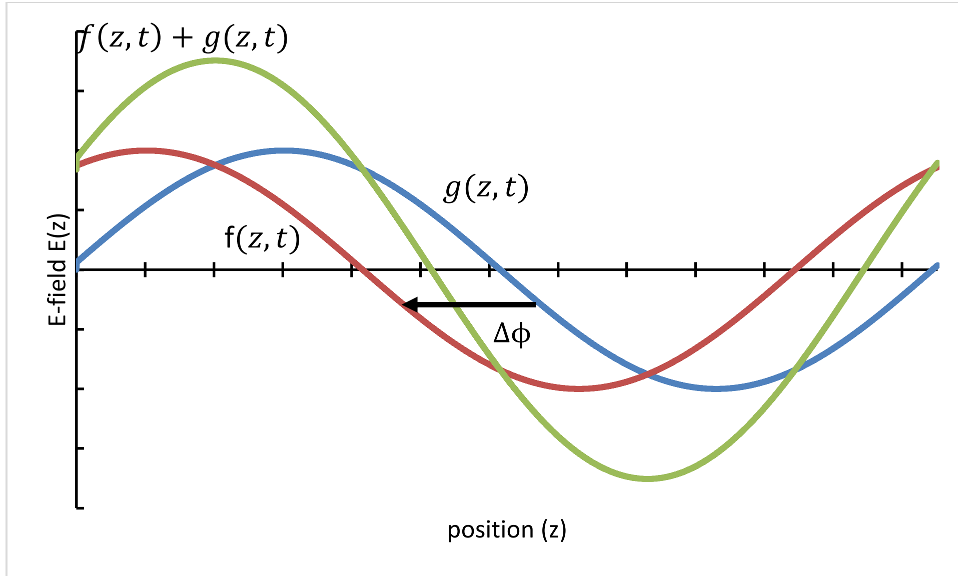

Figure 10. Light Interference. When two electromagnetic waves interfere, the sum creates one wave. The amplitude of this wave is directly dependent on the difference in effective phase shift (Δϕ). If it is close to half of a wavelength, then $f(z,t)$ and $g(z,t)$ destructively interfere, making the resultant wave have a small amplitude. If the phase shift is an integer multiple of the wavelength, the amplitude is at its maximum.

2.2. Determining Film Thickness

When studying the data collected by the interferometer, a series of interference patterns is created and analyzed, such as the one shown in Figure 11. One pixel across all images has an intensity that sinusoidally changes as the mirror of the phase-shifting interferometer moves. To determine the thickness of the film at each pixel, the first step is to model the intensity at each point and determine the effective wave number and effective phase shift.

To model the intensity, start with Equation (34), where

$$\cos^2\left(\frac{\theta}{2}\right) \propto \cos(\theta) + 1 \tag{35}$$

where θ is some constant. The effective phase shifts can be a result of changes to the path length

$$\phi_1 \equiv kz_1 = k(2h_1) \tag{36}$$

and

$$\phi_2 \equiv kz_2 - \frac{\pi}{2} = k(2h_2) \tag{37}$$

where z_1 and z_2 are the changes to the respective path lengths due to a change in position of the mirror surface by h_1 and h_2, respectively from their reference planes.

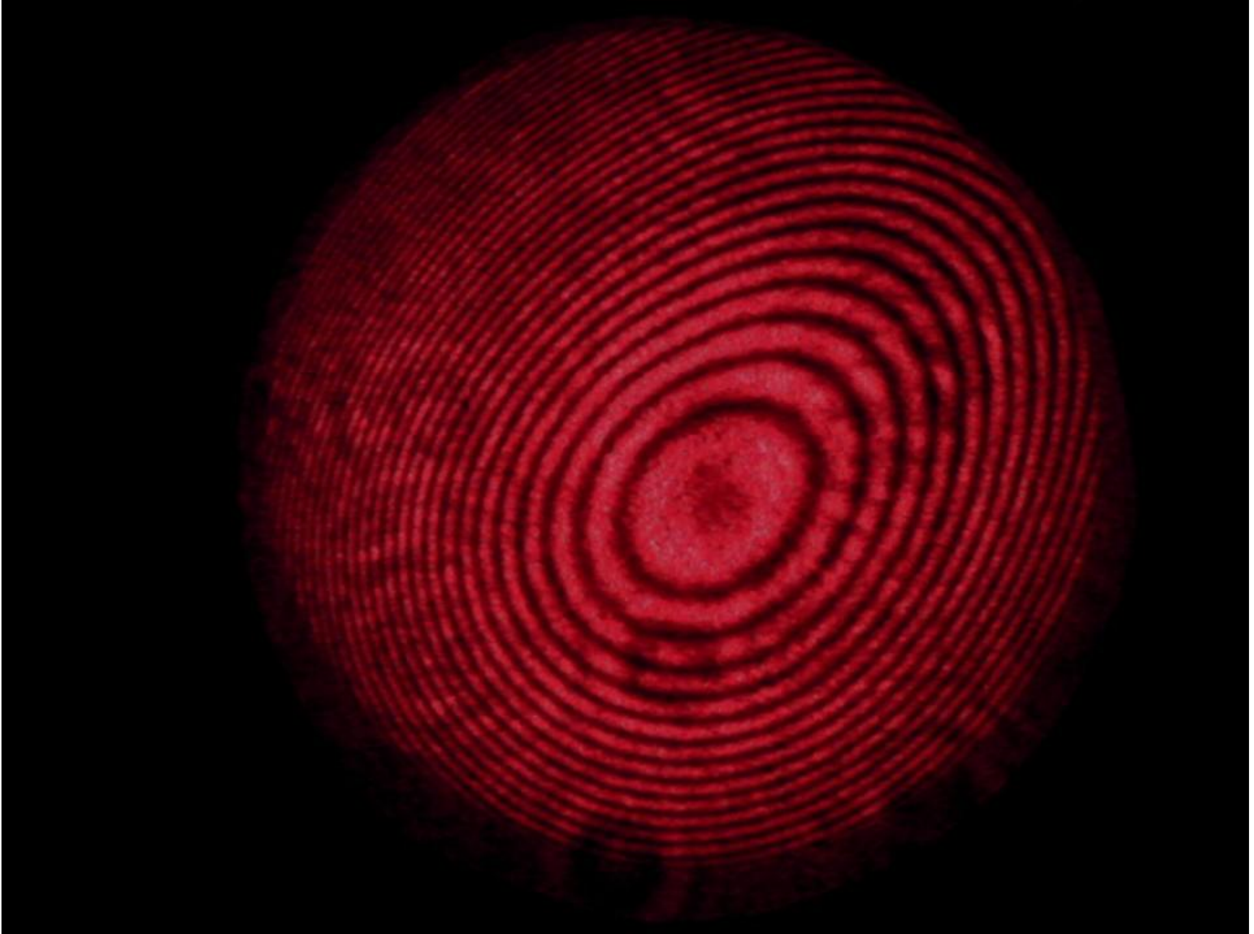

Figure 11. The Interference Pattern. A pattern of bright and dark fringes is created when the light reflecting off the two mirrors meets. A series of these pictures is taken as one mirror shifts, changing the interference pattern. For one point of pixel, the series of points from the images creates an intensity that sinusoidally changes.

In the case of the sample, mirror 1, the change is position-dependent and is due to the surface topography. Notice that a positive topographical feature would results in a negative value of h_1. The subtraction of $\pi/2$ from ϕ_2 is an adjustment to the origin of the reference mirror in order to convert the cosine function into a sine function. The resulting intensity is

$$I \propto \sin(2kh_2 - 2kh_1) + 1. \tag{38}$$

The reference mirror is moved a constant distance δ_i between each image, so that $h_2 = \delta_i i$, where i is the image number (starting with $i = 0$).

The intensity can be modelled as a sine wave where I is the intensity as a function of position (since it depends on the path length difference). Pictures are taken as the mirror moves linearly, so the variable i is used as the position representing the image number. The first image, $i = 0$, is the mirror before it moves, and the image numbers increase as the mirror moves linearly with time. The intensity of one point as the mirror changes is modeled as

$$I(i) = \text{a}\sin(bi - c) + d, \tag{39}$$

where a, b, c and d are all constants that fit the intensity data collected from the interferometer. The model parameters are the intensity amplitude, a, the effective wave number, b, the effective phase shift, c, and the intensity offset, d, which includes any constant background. Specifically,

$$b \equiv 2k\delta_i, \tag{40}$$

and

$$c \equiv 2kh_1. \tag{41}$$

The goal is to determine h_1 for each pixel in the intensity pattern by fitting the model to the intensities of that pixel in all of the images.

2.2.1. Determining the Effective Wave Number

A standard non-linear regression through a Processing code is used to determine the effective wave number of the intensity wave. This method accepts initial guesses for the model parameters, then adjusts them iteratively to minimize the error between the model and the data:

$$\chi^2 = \sum_{i=0}^{N-1} (I_i - a\sin(bi - c) + d)^2 \tag{42}$$

with a, b, c and d being constants. Once χ^2 is limited, the value b is used.

Doing this for every pixel in a set of images is time-consuming, so a simplified analysis has been derived. This analysis assumes that the effective wave number is known and that the number of images included, N, corresponds to a positive integer number, n, of intensity cycles. Therefore, the standard process described above will be conducted on a grid of a few dozen pixels to determine b as a function of the pixel position. The number of images being processed will be

$$N = \frac{n2\pi}{b}. \tag{43}$$

2.2.2. Determining the Effective Phase Shift

Determining the effective phase shift c starts by taking a chi-squared test. This is a test that takes recorded data and subtracts that from the model. This value is then squared. The idea is to make chi-squared as small as possible to minimize the error between the data and the model. The test is conducted with a value expressed as

$$\chi^2 = \sum_{i=0}^{N-1} (I_i - a\sin(bi - c) + d)^2. \tag{44}$$

To minimize χ^2, take the derivative with respect to , then set the derivative to zero and solve for a minimum. Starting with taking the derivative, simplifying gives the relationship

$$\frac{1}{2a}\frac{d\chi^2}{dc} = \sum_{i=0}^{N-1} I_i \cos(bi - c) - \sum_{i=0}^{N-1} a\sin(bi - c)\cos(bx_i - c) - \sum_{i=0}^{N-1} \cos(bi - c). \tag{45}$$

The images are taken at constant intervals over n periods. The sum of an odd function over an integer number of periods equals zero. Thus, the last two terms of Equation (45) will sum to zero. Setting the derivative equal to zero, and using the identity

$$\cos(\alpha - \beta) = \cos(\alpha)\cos(\beta) + \sin(\alpha)\sin(\beta), \tag{46}$$

gives the relationship

$$0 = \sum_{i=0}^{N-1} I_i (\cos(bi)\cos(c) + \sin(bi)\sin(c)). \tag{47}$$

Solving for $\tan(c)$, Equation (47) can be simplified to

$$\tan(c) = \frac{\sin(c)}{\cos(c)} = -\frac{\sum_{i=0}^{N} I_i\, cos(bi)}{\sum_{i=0}^{N} I_i\, sin(bi)}. \tag{48}$$

Taking the numerator and denominator of the right side of Equation (48) and assigning constants to them, such as

$$A = \sum_{i=0}^{N-1} I_i \cos(bi) \tag{49}$$

and

$$D = \sum_{i=0}^{N-1} I_i \sin(bi)\,, \tag{50}$$

then the effective phase shift can be represented as,

$$c = \tan^{-1}\left(-\frac{A}{D}\right). \tag{51}$$

In Equation (39), the intensity of one point versus the positioning of the reference mirror forms a sinusoidal wave. From this equation, the effective phase shift between the reference mirror and the thin film can be determined and is expressed through Equation (51). The relative phase obtained from that is the closest x-intercept of $d\chi^2/dc$, meaning that it is either a minimum or a maximum for χ^2.

The minimum for χ^2 is desired. This occurs when

$$\frac{d^2\chi^2}{dc^2} > 0. \tag{52}$$

The derivative can be taken starting with Equation (45), with the last two terms being equal to zero. It can then be simplified to

$$\frac{D}{2a}\frac{d^2\chi^2}{dc^2} = D^2 - ADtan(c) > 0, \tag{53}$$

and from Equation (48),

$$D^2 + A^2 > 0. \tag{54}$$

This is always true. However, to get Equation (53), both sides of Equation (45) were multiplied by B. If $B < 0$, then the inequality is flipped. Therefore, if $B < 0$, the value of c is calculated from Equation (51) produces a maximum χ^2. Adding π to c will result in a minimum, or the desired effective phase shift of the model. To determine the value of c that corresponds to the height of the sample at that position, each pixel must be compared to its neighbor. Adding a multiple of 2π to the effective phase shift c will leave the intensity model unchanged, so it is added to c to minimize the height difference between adjacent pixels.

2.2.3. Calculation of Film Thickness

The program determining the intensity first determines the height of the pixel at the intersection of the white and yellow lines shown in Figure 12. The yellow line is a bare silicon substrate where no film has been deposited, and the blue line is a thin film that ramps in thickness from zero on one side of the substrate to some maximum thickness on the other. It then proceeds along the white line, comparing each new effective phase shift to that of the previous before determining the new height. Next, it determines the heights of each pixel along the yellow and blue lines, beginning at their respective intersections with the white line. The thickness at any position across the film is the difference between the heights of the blue and yellow lines at that position.

The thickness of the sample will be determined by comparing the height of the bare substrate to the height of the adjacent portion of the film, so that the height is

$$h_1 = \frac{c}{2k}. \tag{55}$$

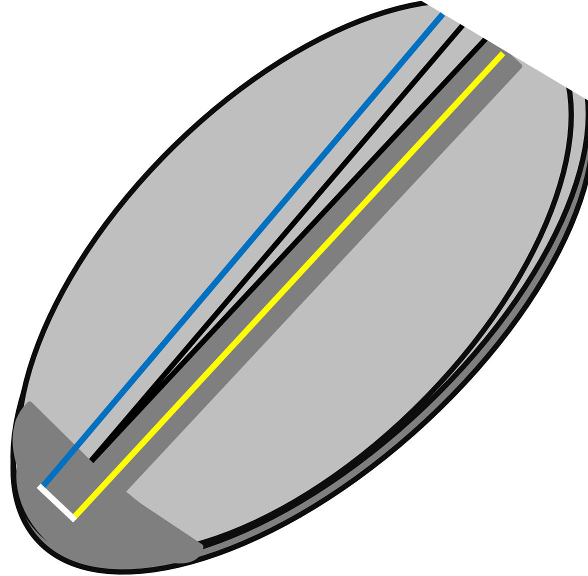

Figure 12. Thin Film sample. A thin film was created so that one side has no film, shown on the bottom left, and the film gradually increases in thickness, shown increasing to the right. A strip of bare silicon substrate goes across the film so that the difference between the bare substrate and the thin film can be measured. The program determining the effective phase shift relates the pixels along the blue and yellow lines, with the blue line going line by line across the thin film to determine the effective phase shift for each point.

Chapter 3

HOUGHTON UNIVERSITY'S INTERFEROMETER

3.1. Houghton University's Phase Shifting Laser Interferometer

Houghton University is developing a modified Twyman-Green phase-shifting interferometer to determine the thickness of thin metal films produced on-site for research purposes. Figure 13 depicts the setup. A 635 nm laser beam diverges with a diverging lens with a focal length of 6 mm, and divides into two beams with a 1-inch cube beam splitter. The beams collimate at 83 mm diameter using converging lenses at a focal length of 500 mm One beam reflects off the 10 cm diameter thin film being studied, while the other reflects off a 10 cm diameter phase-shifting reference mirror. The reference mirror is made to be flat so that the surface error is less than $\frac{1}{10}$ of a wavelength. These beams then return to the beam splitter and combine to show an interference pattern on a semitransparent screen. An HP high-definition camera takes pictures of the interference pattern. It is used in a data processing code to determine the thickness of the sample.

Given ideal optics, perfect alignment, and perfectly flat mirrors, the path length difference between light travelling to a given point on the sample and light travelling to the corresponding point on the phase-shifting reference mirror is the same, even though the actual paths depend on the position of reflection. Therefore, such a situation would produce an interference pattern with uniform intensity.

Figure 14 is a picture of Houghton's interferometer. The setup from Figure 13 sits on a table hanging from four springs. The hanging table limits uncertainty in the data by lessening the effect of shaking from the ground. The table hangs within a metal box with 0.25 x 0.5 x 3 in. neodymium magnets on its walls to create an eddy current as the table moves, limiting the movement of the table even more. The system is also surrounded by blackened walls made of plastic sheets to limit the amount of ambient light picked up by the camera and block the currents made by the air handling system. Before the eddy current damping walls were

installed, the interference pattern would oscillate at about 1-10 periods per second due to the currents. Adding the walls stopped the change in the interference pattern.

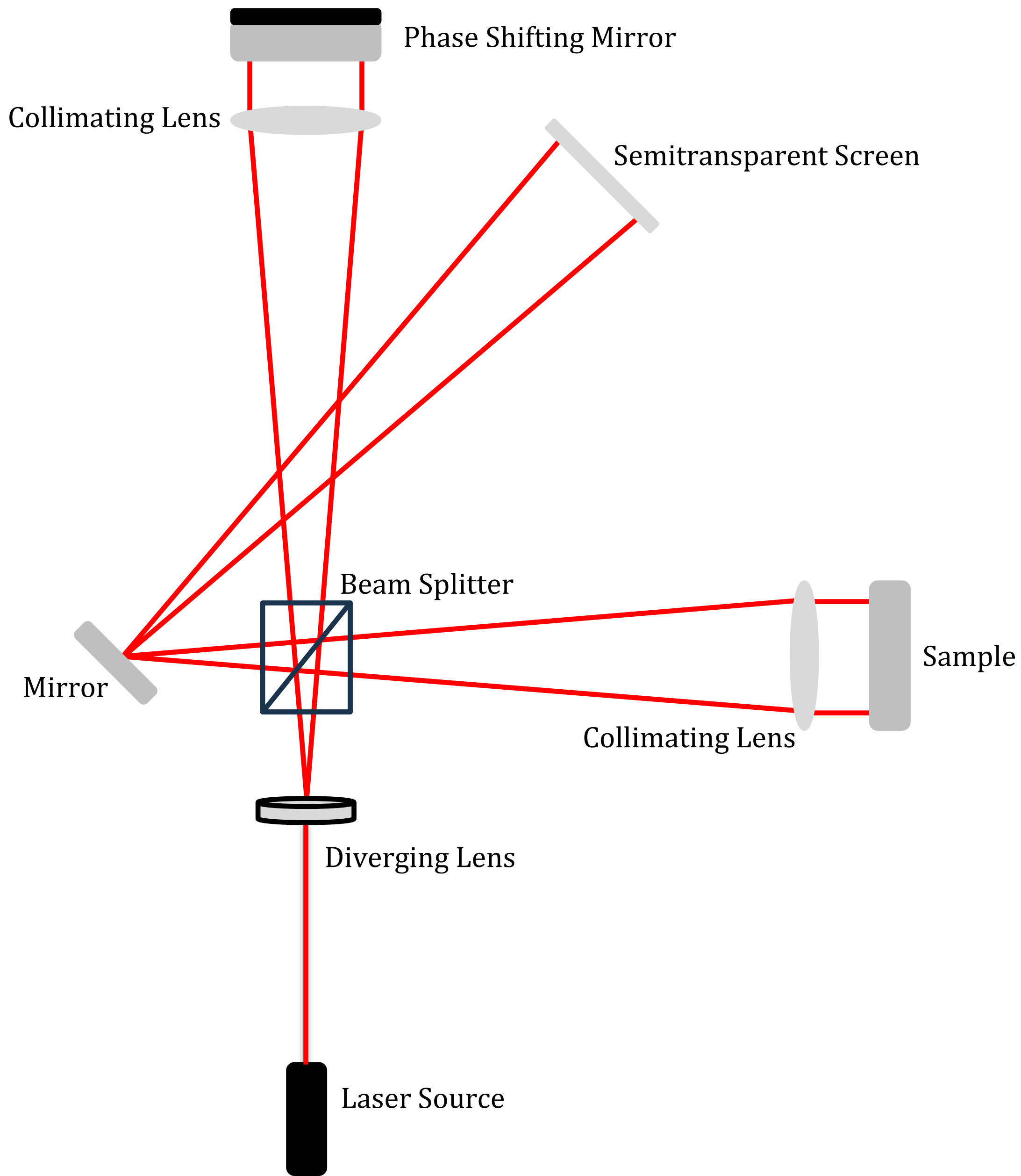

Figure 13. Setup of Houghton's modified Twyman-Green Interferometer. The laser source emits a 635 nm beam that is then diverged and split into two beams. One beam is reflected off the thin metal film sample being studied after being collimated at 10 cm. The other beam is collimated at 10 cm and then reflected off a flat, phase-shifting reference mirror. The beams are then joined back together, and an interference pattern is shown on the screen.

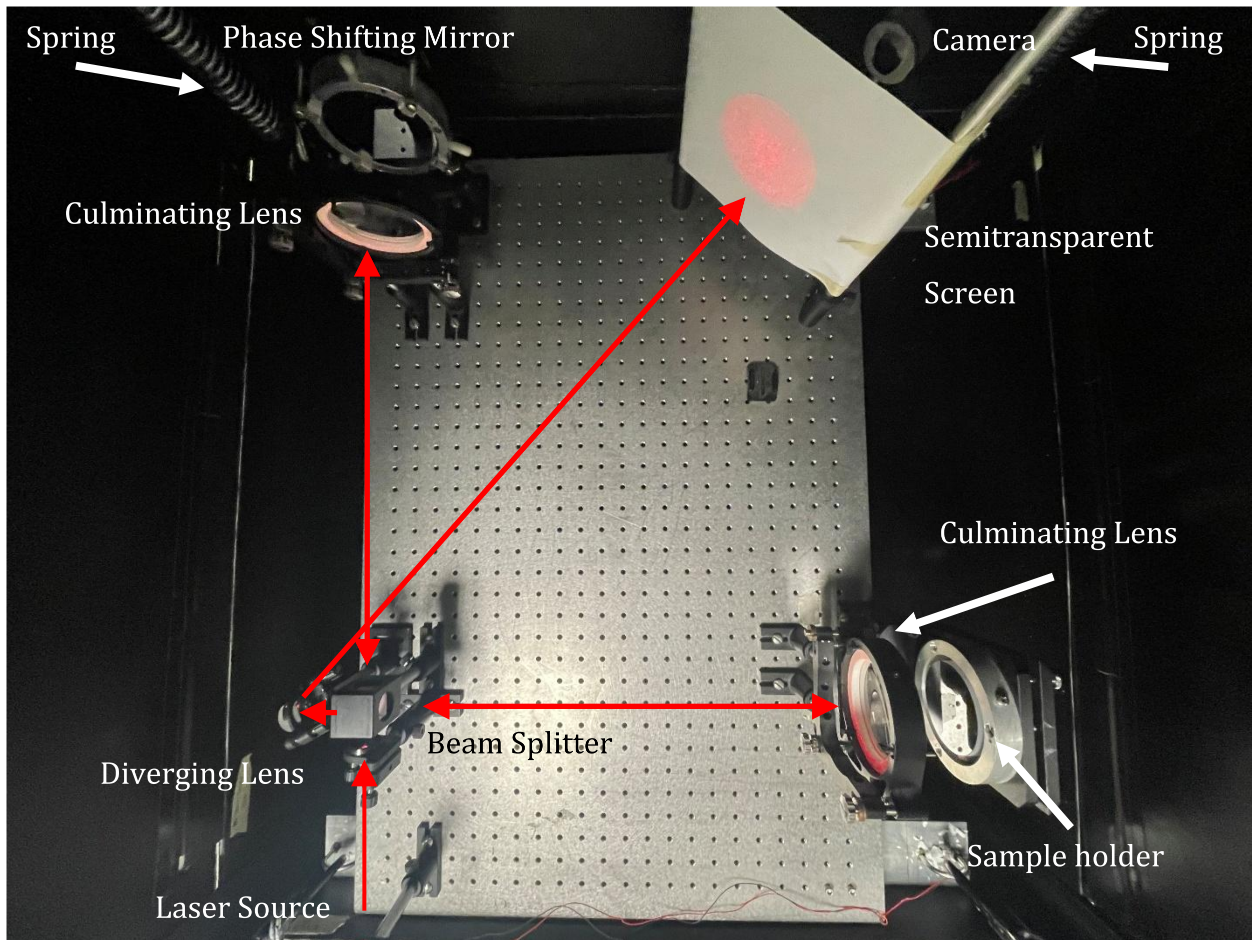

Figure 14. Houghton University's Interferometer. The setup is on a table surrounded by current-damping walls that block current and limit the ambient light that the camera picks up when it takes pictures of the interference pattern. The table is suspended by four springs that reduce the effect of vibrations in the room moving the table. Magnets on a block surrounding the table are installed to create eddy currents when the table moves,

3.2. Phase Shifting Mirror

3.2.1. Hardware

The phase-shifting mirror, depicted in Figure 15, moves between images being taken of the interference pattern. The phase shift changes between images, and thus the interference pattern changes. Three piezoelectric actuators (piezo) move the reference mirror by deforming when a voltage is applied. At a higher voltage, the piezo contracts, becoming skinnier and longer, moving the mirror further away from the stand that it is clamped to. The applied voltage is regulated using an Arduino.

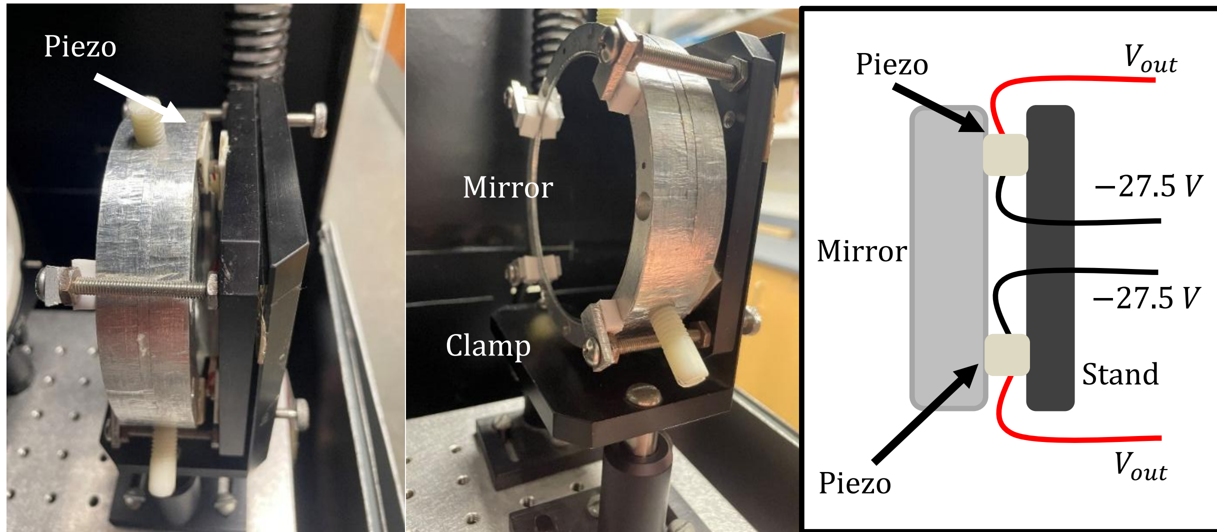

Figure 15. Reference Mirror. The three piezoelectric actuators compress up and down and stretch left and right, changing the position of the reference mirror when a voltage is applied across it. The $\sim 60\ V$ difference in potential results in the mirror moving a couple of micrometers, meaning 3 periods are seen.

3.2.2. Ramp Circuit

The voltage applied to the piezoelectric ceramics starts at 0 V and increases linearly until the voltage across the piezo is 60 V. The circuit has three parts: An Arduino outputs a PWM signal with an average voltage that increases linearly from 0 to 5 V, a dual-stage low-pass filter that smooths out the voltage, and finally, an amplifier to increase the voltage to the desired range. Figure 16 explains the circuit created to ramp up the voltage. The dual-stage low-pass filter and amplifier are both floating at 2.5 V so that the relative PWM voltage oscillates between -2.5 to 2.5 V. The amplifier outputs $-30\ V$ to 30 V relative to its 2.5 V reference. The output that is then connected to the phase-shifting mirror has the positive end connected to V_{out} and the negative end connected to the $-27.5\ V$ power supply.

3.2.3. The Interference Pattern

The three piezos move the phase-shifting reference mirror such that the light intensity of a given spot on the interference pattern goes through 3 cycles. This is all captured on the HP high-definition camera between steps that the piezo takes. The sinusoidal intensity change is partially expressed through Figure 17, where the pixel's intensity pattern is formed from the interferometer's trial run changes throughout the photos.

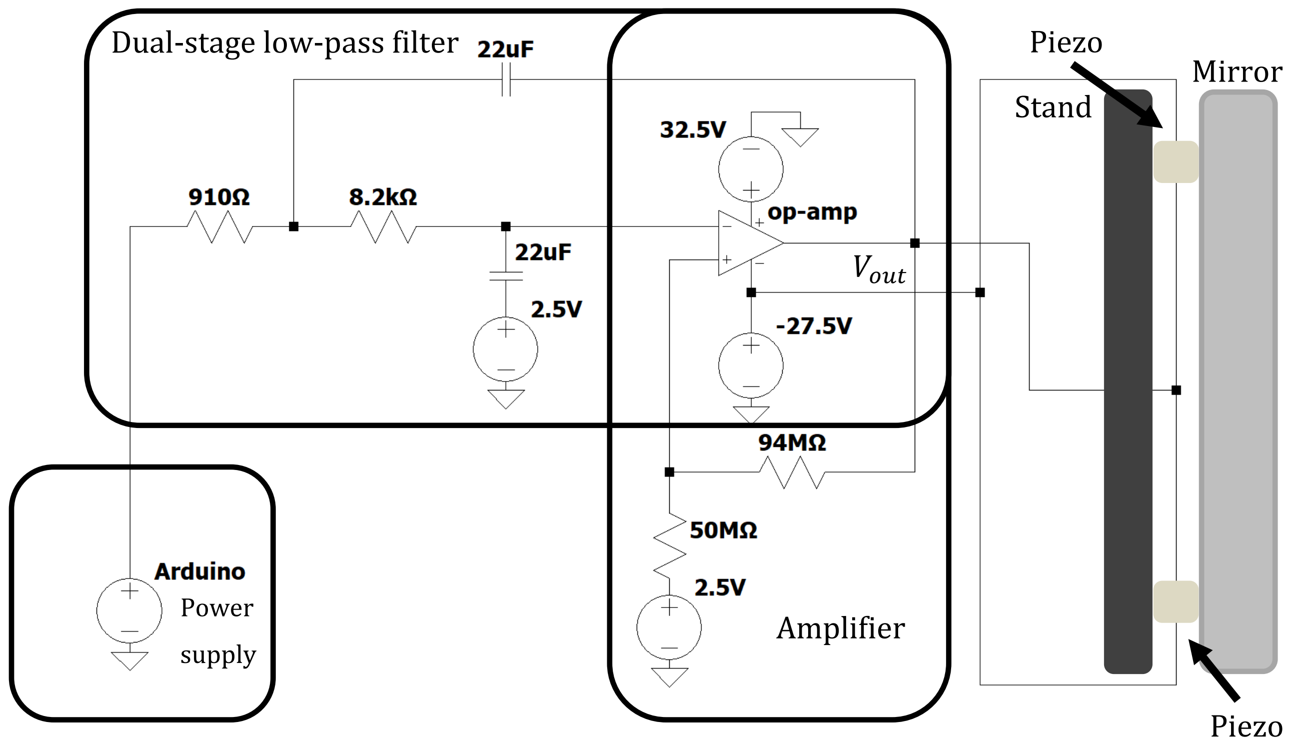

Figure 16. Systematic Diagram of the ramp circuit. An Arduino outputs a PWM signal with an average voltage that increases linearly from 0 V to 5 V. The filter is floating at 2.5 V and then smoothed and amplified so that 0 V to 57.5 V by a dual-stage low-pass filter.

3.3. Data Analysis Code

3.3.1. Determining Intensity

Focusing on one point on the thin film and studying the intensity of the point on the interference pattern in the series of images gives a sinusoidal relationship between the position of the mirror and the intensity of that one point, as shown in Figure 18. The mirror position is represented as the image number, where $i = 0$ has no potential across the piezos, and image 99 is taken when there is 60 V across them. To determine the intensity of each pixel for each image, the pictures are downloaded onto a Processing code, which uses an RGB intensity model to give relative luminance for each point. The data is then put into Excel to create a scatterplot.

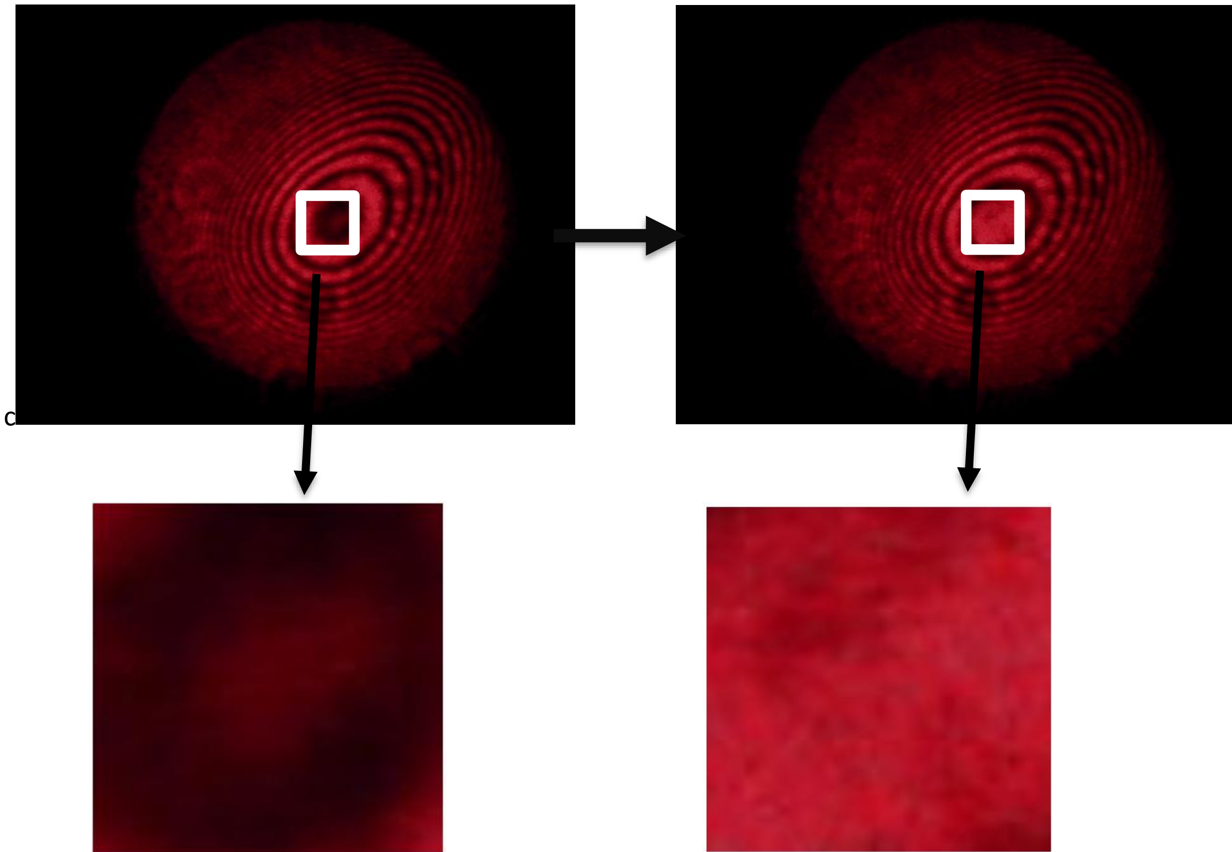

Figure 17. Changing the interference pattern as the mirror shifts. This diagram is two pictures shown at difference mirror positions. As the phase-shifting mirror moves, the interference pattern shown on the screen changes at each pixel.

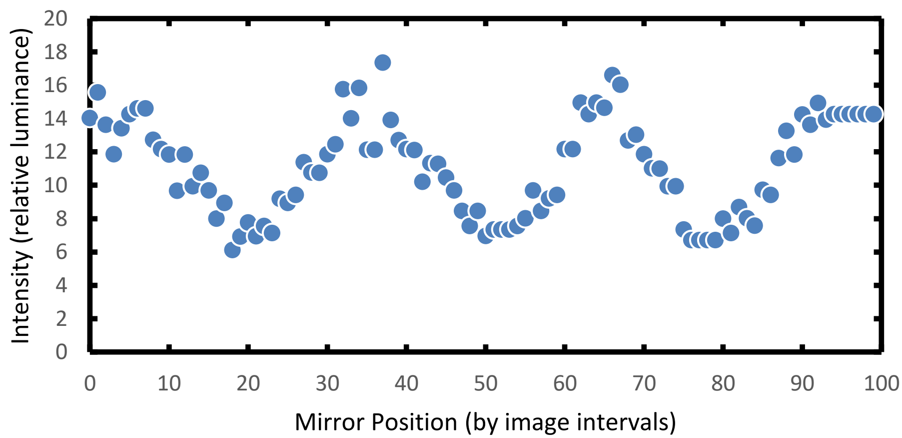

Figure 18. Intensity vs. image. The sinusoidal relationship between the images – taken periodically throughout the movement of the mirror – is depicted between intensity and image. The intensity changes sinusoidally as the mirror position changes.

3.3.2. Finding the Effective Phase Shift

A Processing code was written to determine the intensity at each point on each image and use those intensities to find the phase shift in the data. This shift is a representation of the path length difference the light had to travel between the reference mirror and the sample. When started, the program applies a voltage across a user defined amount of time while periodically taking a user defined number of photos. The photos are then loaded into a 3D array that holds the intensity of each pixel on each image. This array is used to model a sine wave for all desired pixels using the series of images.

For a thin metal film depicted in Figure 12, the user can choose a line of pixels, then the program will start at the point with the thinnest film, and determine the effective phase shift according to Equation (51) over the number of images determined through Equation (43). From that, the program will determine the thickness by relating the pixels effective phase shift to the that if the bare substrate row subsequent to it. Finally, using Equation (55), the height difference between the film and the bare substrate point is determined for that pixel. The program will then move onto the next pixel and continue the process until each pixel on the series of images is analyzed.

Chapter 4

CONCLUSION

In conclusion, Houghton University created a phase-shifting laser interferometer for the study of thin metal films. Images of an interference pattern using a straight silicon substrate were taken. A Processing code was made to determine the thickness of each point on the thin metal film. The images have not been used yet to determine thickness; however, a phase shift has been determined for each point on a data set. The uncertainty in our calculations also still needs to be measured. In the future, Houghton University plans on using a thin metal film to measure its thickness using the interferometer and write a code to determine the uncertainty in the measurement of the thickness.

R e f e r e n c e s

[1] I. Newton, *Opticks or a Treatise of the Reflexions, Refractions, Inflexians and Colours of Light*. (Dover Publications, New York, 1952).
[2] H. Hertz, *Ueber einen Einfluss des ultravioletten Lichtes auf die electrische Entladung*. *Annalen der Physik* (1887).
[3] A. Einstein, *On the electrodynamics of moving bodies.* (1905).
[4] C. Huygens, *Treatis on Light.* (Pierre Van der Aa, Leiden, 1690).
[5] R. Hooke, *Micrographia: Or Some Physioloical Descriptions of Minute Bodies Made by Magnifying Glasses. (*Royal Society, London, 1665).
[6] J. C. Maxwell, "A dynamical theory of the electromagnetic field," *Philos. Trans. R. Soc. Lond.* **155**, 459–512 (1864).
[7] J. C. Maxwell, *On physical lines of force*. *Philosophical Magazine* (1861).
[8] M. Faraday, "Experimental Researches in Electricity," *Philos. Trans. R. Soc. Lond.* **122**, 125–162 (1832).
[9] C. A. Coulomb, "Premier mémoire sur l'électricité et le magnétisme," *Hist. Acad. R. Sci.* 569–577 (1785).
[10] A. M. Ampère, "Sur l'action mutuelle de deux courants électriques," *Annales de Chimie et de Physique* **15**, 59–76 (1820).
[11] C. F. Gauss, "Allgemeine Lehrsätze in Beziehung auf die im verkehrten Verhältnisse des Quadrats der Entfernung wirkenden Anziehungs- und Abstoßungskräfte," *Werke* **5**, 197-244 (1867).
[12] T. Young, "The Bakerian Lecture: Experiments and Calculations Relative to Physical Optics," Philos. Trans. R. Soc. Lond. **94**, 1–16 (1804).
[13] A. A. Michelson, "On the relative motion of the Earth and the luminiferous ether," *Am. J. Sci.* **22**, 120-129 (1881).
[14] R. S. Shankland, "Michelson and his Interferometer," Phys. Today **27**, 37-43 (1974).
[15] M. S. Belsley, "The Michelson Interferometer: A Tool for Measuring the Speed of Light," Phys. Teach. **41**, 464-467 (2003).
[16] F. Twyman, "an interferometer for testing camera lenses," Trans. Opt. Soc. Lond. **22**, 174-193 (1921).
[17] F. Twyman, "The Testing of Microscope Objectives and Microscopes by Interferometry," Proc. Phys. Soc. Lond. 16, 208 (1920).
[18] A. J. Lewis, "Absolute length measurement using multiple-wavelength phase stepping interferometry," *Ph.D. thesis, University of London* (1993).
[19] P. Sonnweber-Ribic, P. A. Gruber, G. Dehm, H. P. Strunk, E. Arzt, "Kinetics and driving forces of abnormal grain growth in thin Cu films," Acta Materialia **60**, 2397-2406 (2012).
[20] S. P. Baker, B. Hoffman, L. Timian, A. Silvernail, E. A. Ellis, "Texture Transformations in Ag thin films," *J. Mater. Sci.* **48**, 7121-7132 (2013).